ABSTRACT

An adjoint sensitivity analysis of the RAS scheme in NASA's GEOS-1 GCM with respect to perturbations in large-scale environmental fields was conducted. The response functions were defined as measures of the strength of convective cloud precipitation, the cloud-induced heating and drying (moistening) in both instantaneous and time-integrated sense. The roles of different variables in producing variations on the response functions were evaluated and the most sensitive vertical levels of the perturbations were identified with the gradient provided by the adjoint model.

It was found that the potential temperature perturbations had significant impact on all the response functionals analyzed, especially on the convective precipitation. The perturbations at subcloud layers and at mid-troposphere from 500 to 600 hPa were found to be the most influential. The impact from the moisture fields was most significant on cloud heating and drying effects and the strongest influence came from the subcloud layers. The moisture perturbations at mid-troposphere also significantly influenced the cloud drying (moistening) effect. On the other hand, the cloud-induced heating and drying at levels between 400 and 600 hPa felt the strongest impact from perturbations in large-scale fields. The influence of the perturbations in the wind field was weaker but still provided reasonable sensitivity patterns.

The sensitivity analysis results obtained indicated that accurate grid-scale vertical profile of temperature and moisture, especially at subcloud layers and mid-troposphere between 500 to 600 hPa were essential for the accurate evaluation of the cumulus cloud effects. The implications of the results of this work for variational data assimilation were also discussed.

1 INTRODUCTION

The heating and moistening(drying) induced by convection clouds play an important role in the energy balance and water budget in the global atmosphere, therefore the representation of the effects of convective clouds is recognized as a key process in numerical weather prediction for time scales ranging from short-term forecasting to seasonal prediction and climate simulation. Moreover an accurate parameterization of sub-grid moisture processes in a general circulation model (GCM) is essential to fully assimilate such observational data as precipitation, cloudness and outgoing radiation which are closely related to moisture and convection.

The Goddard Earth Observing System-1 (GEOS-1) GCM was developed by the Data Assimilation Office (DAO) at NASA/GSFC/Goddard Laboratory for Atmospheres (GLA) in collaboration with the Climate and Radiation Branch (for details please refer to Takacs et al, 1994). It is currently used in conjunction with an analysis scheme to produce a multi-year global atmospheric data set for climate research. It has also been used to produce multiple 10-year climate simulations.

There are four physics packages in the GEOS-1 GCM, namely the RAS parameterization and large-scale convection schemes, the short-wave radiation and long-wave radiation schemes, and the turbulence parameterization scheme, respectively. Among them the moist process plays an essential role towards improving the quality of the products of the Data Assimilation System (DAS). The Relaxed Arakawa-Schubert (RAS) parameterization scheme (Moorthi and Suarez, 1992) is the central part of the moisture processes.

RAS is a parameterization of sub-grid cumulus convection in terms of the large-scale fields. It computes the cloud-induced variatons in potential temperature θ and moisture q as well as convective precipitation according to large-scale conditions in θ and q. Those outputs impact on the large-scale fields and in turn the modified environmental conditions influence the cloud activities. To improve the model forecast and the quality of data assimilation products, a thorough understanding of the interactions between large-scale fields and convective clouds in the model and an evaluation of the performance of the parameterization scheme in terms of its sensitivity to the large-scale environmental fields are indispensable prerequisites. The present work represents an effort toward this goal.

In a sensitivity study a gradient of certain measure of model output (response function) is calculated with respect to perturbations in the model input variables and parameters. There are two approaches to calculate the gradient. One consists of the conventional forward sensitivity analysis, also called the perturbation method. In this algorithm, a series of experiments are carried out, each with one parameter or one state variable at one grid point being perturbed, then the variations in the response function produced by each of them are compared. Obviously, for large dimensional systems in question, this approach is computationally prohibitive.

The other approach is the adjoint (backward) sensitivity analysis (see Cacuci(1988) for a review). It provides an efficient way for calculating the gradient by a single integration of the adjoint model and is particularly suitable for the problems in atmospheric and oceanic models with large dimensions and relatively few responses. It has been successfully applied to a wide range of sensitivity problems, for example, the sensitivity to model parameters by Hall et al(1982), Hall(1986), Rinne and Järvinnen(1993), the sensitivity of blocking processes by Zou et al(1993), the sensitivity of one forecast aspects to initial conditions by Rabier et al(1992) and Rabier et al(1996). It also has been used in parameter estimation (Navon, 1997). Another related work is that by Fillion and Errico(1997), in which some basic aspects related to the problem of incorporating moist convective processes in a variational data assimilation framework are addressed.

In the present work an adjoint sensitivity study is carried out to evaluate the impact of grid-scale perturbations on RAS output both qualitatively and quantitatively. The following issues are addressed:

- Examining the spacial variation of the sensitivity and identifying the vertical levels where the perturbations have the largest impact on RAS output;

- Evaluating the relative importance of the perturbations in the temperature, moisture and wind fields of the surrounding air in changing the outputs of RAS scheme;

- Discussing the feedback between the convective clouds and the large-scale fields.

The outline of this article is as follows. In section 2, we describe the theory and algorithm of adjoint sensitivity. Section 3 consists of a brief description of the RAS scheme in the GEOS-1 GCM. Section 4 presents an analysis of the results of the sensitivity analyses. Summary, conclusions and the implications of this work for further research are provided in section 5.

2 Adjoint sensitivity method

In sensitivity analysis, we first define a response function R, which is a measure of the forecast aspects we are interested in. Here we only consider the functional type of response, i.e. R is a real scalar:

$$R = R(\mathbf{x}, \alpha)$$

where $\mathbf{x}$ is the vector consisting of all the model state variables over all the model gridpoints and α is the vector of all the model parameters. We aim at evaluating the sensitivity of the change of R with respect to changes in $\mathbf{x}$ and α. Specifically, we are concerned with the impact of small changes in the surrounding air on the output of RAS scheme, since these outputs will in turn affect the large-scale environmental fields which are directly relevant to the model forecast.

Let $\mathbf{y} = \mathbf{A}(\mathbf{x}, t)$ represent the output vector of RAS scheme, where $\mathbf{x}$ is the vector consisting of the large-scale environmental fields which are inputs of RAS scheme and $\mathbf{A}$ represents the nonlinear RAS operator. The following three general types of response functionals ((a) to (c)) are considered:

$$(a) \qquad R_1 =< \mathbf{y}, \mathbf{y} >_{\mathbf{S}} = \mathbf{y}^T \mathbf{S} \mathbf{y} \tag{1}$$

where $< \cdot\ ,\ \cdot >_{\mathbf{S}}$ stands for the inner product between two vectors weighted by a real, symmetric matrix $\mathbf{S}$ specified according to the field of interest, $(\ )^T$ stands for transpose.

$$(b) \qquad R_2 =< W, \mathbf{y} >_{\mathbf{E}} = W^T \mathbf{y} \tag{2}$$

Here W is a specified weighting vector and $< \cdot\ ,\ \cdot >_{\mathbf{E}}$ is a normal Euclidean inner product. The above two functionals are viewed as instantaneous responses, i.e. they are for one time level which is the same as that of the input variables. We can also define a time-integrated response as:

$$(c) \qquad R_3 = \int_{t_0}^{t_N} < \mathbf{y},\ \mathbf{y} >_{\mathbf{S}} dt = \int_{t_0}^{t_N} \mathbf{y}^T \mathbf{S} \mathbf{y} dt \tag{3}$$

a. *Instantaneous sensitivity*

To determine the impact of small perturbations in the surrounding air on R, we need to evaluate the gradient of R with respect to the input $\mathbf{x}$. By using a Taylor expansion and retaining only the first-order approximation, a small perturbation $\delta \mathbf{x}$ on the state vector causes a change δR_1 in the response function that can be calculated by

$$\begin{aligned} \delta R_1 &= 2 < \mathbf{y}, \delta \mathbf{y} >_{\mathbf{S}} \\ &= 2 < \mathbf{y}, \frac{\partial \mathbf{A}(\mathbf{x}, t)}{\partial \mathbf{x}} \delta \mathbf{x} >_{\mathbf{S}} \\ &= 2 \mathbf{y}^T \mathbf{S} \left[\frac{\partial \mathbf{A}(\mathbf{x}, t)}{\partial \mathbf{x}} \delta \mathbf{x} \right] \\ &= 2 \left\{ \left[\frac{\partial \mathbf{A}(\mathbf{x}, t)}{\partial \mathbf{x}} \right]^T \mathbf{S}^T \mathbf{y} \right\}^T \delta \mathbf{x} \\ &= 2 < \left[\frac{\partial \mathbf{A}(\mathbf{x}, t)}{\partial \mathbf{x}} \right]^T \mathbf{S}^T \mathbf{y}, \delta \mathbf{x} >_{\mathbf{E}} \end{aligned} \tag{4}$$

where $\partial \mathbf{A}(\mathbf{x}, t)/\partial \mathbf{x}$ is the Jacobian representing the tangent-linear operator of the RAS scheme. Its adjoint is simply its transpose

$$\left[\frac{\partial \mathbf{A}(\mathbf{x}, t)}{\partial \mathbf{x}}\right]^T .$$

From (4) we can see that the gradient of R_1 with respect to $\mathbf{x}$ is:

$$\begin{aligned} \bigtriangledown_{\mathbf{x}} R_1 &= 2\left[\frac{\partial \mathbf{A}(\mathbf{x}, t)}{\partial \mathbf{x}}\right]^T \mathbf{S}^T \mathbf{y} \\ &= 2\left[\frac{\partial \mathbf{A}(\mathbf{x}, t)}{\partial \mathbf{x}}\right]^T \mathbf{S}\mathbf{y} \end{aligned} \tag{5}$$

In practice, this can be obtained by first running the original RAS with prescribed large-scale conditions at a certain time t to obtain $\mathbf{y} = \mathbf{A}(\mathbf{x}, t)$, multiply it by $\mathbf{S}$, then take the result as the input to the adjoint of RAS. The output of the adjoint of RAS yields the gradient vector. The component of the vector corresponding to each of the variables is the gradient of R_1 with respect to that particular variable.

For the R_2 response, a similar reasoning as above leads to :

$$\bigtriangledown_{\mathbf{x}} R_2 = \left[\frac{\partial \mathbf{A}(\mathbf{x}, t)}{\partial \mathbf{x}}\right]^T W \tag{6}$$

Therefore the input to the adjoint of RAS is the weighting vector W instead of $\mathbf{S}\mathbf{y}$ for R_1.

b. *Time-integrated sensitivity*

The perturbation of the R_3 response is derived as above and can be expressed as:

$$\delta R_3 = 2\int_{t_0}^{t_N} < \left[\frac{\partial \mathbf{A}(\mathbf{x}, t)}{\partial \mathbf{x}}\right]^T \mathbf{S}^T \mathbf{y}, \delta \mathbf{x} >_{\mathbf{E}} dt \tag{7}$$

We need to evaluate the gradient of R_3 with respect to the initial perturbations $\delta \mathbf{x}_0 = \delta \mathbf{x}|_{t=t_0}$. Recall that a small perturbation $\delta \mathbf{x}(t)$ can be related to $\delta \mathbf{x}_0$ through the resolvent $\mathcal{L}(t, t_0)$ of the tangent-linear model of the GCM:

$$\delta \mathbf{x} = \mathcal{L}(t, t_0) \delta x_0 \tag{8}$$

Defining $\mathcal{L}^*(t_0, t)$ as the adjoint of $\mathcal{L}(t, t_0)$, δR_3 may be written as

$$\delta R_3 \quad = \quad < 2\int_{t_0}^{t_N} \left\{ \mathcal{L}^*(t_0, t) \left[\frac{\partial \mathbf{A}(\mathbf{x}, t)}{\partial \mathbf{x}}\right]^T \mathbf{S}^T \mathbf{y} \right\} dt, \delta \mathbf{x}_0 >_{\mathbf{E}} \tag{9}$$

Therefore the gradient of R_3 with respect to initial perturbation is given by

$$\bigtriangledown_{\mathbf{x_0}} R_3 = 2\int_{t_0}^{t_N} \left\{ \mathcal{L}^*(t_0, t) \left[\frac{\partial \mathbf{A}(\mathbf{x}, t)}{\partial \mathbf{x}}\right]^T \mathbf{S}^T \mathbf{y} \right\} dt \tag{10}$$

By definition, in areas with large gradient, a perturbation $\delta \mathbf{x}_0$ would create a larger impact on R_3 than the same perturbation in areas with small gradient. Thus the 3-D distribution of this gradient provides the sensitivity pattern of R_3 to $\mathbf{x}_0$. Also this gradient yields the optimal initial perturbation pattern in the sense that for all the initial perturbations with given value of the norm $\|\mathbf{x}_0\|$, the one with the same spatial distribution as $\bigtriangledown_{\mathbf{x_0}} R_3$, i.e., parallel to $\bigtriangledown_{\mathbf{x_0}} R_3$ in phase space, imposes the largest changes in R_3. The same argument applies to the gradients of R_1 and R_2. In the present paper we use the terms gradient and sensitivity interchangeably.

In practice, the algorithm to calculate the gradient vector (10) is as follows:

1. Integrate the GCM from time $t = t_0$ to $t = t_N$, saving the environmental fields as well as the RAS output [$\mathbf{y}$ in (10)] at times t_n, for $n = 0, 1, 2, \ldots, N$;

2. At each time t_n, use the stored trajectory of RAS [$\mathbf{y} = \mathbf{A}(\mathbf{x}, t)$] and the adjoint RAS to calculate (5) to obtain the gradient of R with respect to instantaneous perturbations of the large-scale fields at each time t_n;

3. Finally, integrate backward in time the adjoint of the GCM from t_N to t_0, with the result of step 2 at t_N as the initial condition. Since $\mathcal{L}^*$ is linear, the result of step 2 is added to the corresponding environmental fields of the adjoint GCM at each t_n. The result at t_0 is $\bigtriangledown_{\mathbf{x_0}} R_3$ in (10).

Note that while (5) provides the sensitivity of the response with respect to instantaneous perturbation in the surrounding air, the integration of the adjoint of the GCM yields the time evolution of sensitivity.

From the above we can see that the merit of the adjoint method lies in that a single adjoint model integration yields the gradient of one response function to all the model variables at all model grid points. If instead we were to use the forward direct sensitivity method, then to obtain the same information would require to integrate the original model $N \times M$ times, where N is the number of variables and M is the number of model grid points (on the order of 10^5). This is computationally prohibitive even with the most powerful computers available today.

In what follows W and $\mathbf{S}$ are chosen to define different response functionals in order to examine various aspects of RAS sensitivity.

3 The RAS parameterization scheme in GEOS-1 GCM

RAS is a parameterization of sub-grid scale penetrative and shallow cumulus convection in terms of large-scale fields (Moorthi and Suarez, 1992). It predicts mass fluxes from cloud types which have different entrainment rates and levels of neutral buoyancy, depending on the properties of the large scale environment. In this scheme, all clouds are assumed to have the same base but each cloud type is characterized by its detrainment level (cloud top). The normalized mass flux for each cloud type is a linear function of height. In the original Arakawa-Schubert scheme, the closure assumption is a balance between large-scale and grid-scale effects on the cloud work function which is a measure of efficiency of convection. In RAS, the major simplification is to 'relax' the state toward equilibrium each time the parameterization is invoked, rather than requiring that the final state be balanced.

At each model time step, several different cloud types are treated sequentially. At any instant, each cloud feels only the 'current environment' which results from DT the effect of the previous cloud type in the sequence. In this way, the interactions between clouds are accounted for implicitly. The effect of re-evaporation of the falling rain is also taken into account.

The adjoint of the adiabatic GCM and the RAS scheme were developed and documented in Yang and Navon (1996) and Yang et al. (1997) . In the present study the RAS scheme is the only physical process included in the GCM and its adjoint model.

All the experiments were performed with a $5^0 \times 4^0$ horizontal resolution on 20 vertical σ levels. The initial time is arbitrarily chosen at 00GMT, Jan. 1st, 1985. The initial data is extracted from the DAO archived data set which is assimilated and analyzed with the data assimilation system of DAO. It has the same resolution as the model and includes five independent variables, namely the potential temperature, the zonal and meridional wind, the surface pressure and the specific humidity, respectively. The time integration was carried out for 6 hours.

To provide a brief idea of the effect of convective clouds on large-scale environment and to better understand the sensitivity analysis results, some outputs from RAS scheme are discussed here.

Fig.1a shows the convective cloud precipitation from RAS at the initial time. It indicates that strong convective activities occur over the low latitude oceans, especially over the eastern Indian and the western Pacific Oceans as well as the Atlantic Ocean.

Fig.1b is the longitude-height distribution of the rate of convection-induced potential temperature change $\Delta\theta$, averaged between 10^0S and 10^0N. The ordinate is the vertical σ level. It indicates that convective clouds act as a heat source to the environmental air at all levels . The strongest heating occurs at the mid-troposphere between $\sigma = 0.4$ and $\sigma = 0.5$ (between 400 and 500 hPa). Longitudinally, the Indian and Western Pacific Oceans are the areas with the strongest convective heating. The levels between $\sigma = 0.1$ and 0.2 (around 100 to 200 hPa) also exhibit very strong heating rate. This feature is probably due to the fact that here the heating rate is calculated by the change of $\Delta\theta$ in unit time. To be converted into an actual temperature change ΔT, $\Delta\theta$ should be multiplied by a factor $(p/p_0)^\kappa$, where p is the pressure and p_0 is a reference pressure, $\kappa = R/C_p$, where R is the gas constant and C_p is the specific heat at constant pressure.

Therefore the heating at the higher levels is scaled down more than at the lower levels. Throughout this paper the heating rate is represented by $\Delta\theta$ rather than by ΔT.

Fig.1c is the rate of cloud-induced moisture change Δq. Only the layers below $\sigma = 0.3$ are shown. The convective cloud generally dries out the layers below 500 hPa, especially the subcloud layers and around 600 hPa, but only weakly moistens the upper layers. At mid-troposphere, the layer with the strongest convective drying is lower than that with the strongest heating.

The convective clouds impact upon the large-scale fields through $\Delta\theta$ and Δq. On the other hand, variations in grid scale vertical profile in the environing air, in turn, influence the convective activities. In the following sections we will investigate the sensitivity of the RAS outputs to large scale environmental fields, i.e. how small perturbations in the surrounding air induce changes in the RAS outputs.

All the gradients obtained using the adjoint model were subject to a gradient correctness test. The following function is calculated:

$$F(\beta) = \frac{R(\mathbf{x} + \beta h_{\mathbf{x}}) - R(\mathbf{x})}{< \bigtriangledown_{\mathbf{x}} R,\ \beta h_{\mathbf{x}} >_E} \tag{11}$$

where $h_{\mathbf{x}}$ is a prescribed distribution of perturbation and β is a scaling factor which controls the magnitude of the perturbation. Here $h_{\mathbf{x}}$ is obtained by taking the difference between the result of a 6 hour integration of the original GCM and the initial condition. Within several orders of magnitude of β, a unit value of $F(\beta)$ is obtained. As an example, Table 1 provides the result of the gradient check for one of the response functionals. It indicates the range of the validity of the adjoint sensitivity.

4 Sensitivity Analysis Results

a. *Instantaneous sensitivity*

In this subsection we present the results of instantaneous sensitivity, i.e. the response functionals are for a single time-level.

Table 1: result of the gradient test

β	$F(\beta)$
1.0×10^{0}	1.075056131
1.0×10^{-1}	1.001115046
1.0×10^{-3}	1.000012075
1.0×10^{-5}	1.000000098
1.0×10^{-7}	0.9999898195
1.0×10^{-9}	1.000668568
1.0×10^{-11}	0.9696400849

1) CONVECTIVE PRECIPITATION

Here the response functional is defined as:

$$R_p = \sum_{\Omega} P_r$$

where P_r is the convective cloud precipitation rate. Ω is the low-latitude belt from 30^0S to 30^0N, where most of the precipitation occurs.

Fig.2a shows the longitude-vertical distribution of the sensitivity of precipitation to θ field, averaged between 10^0S and 10^0N. A large positive sensitivity is observed below the cloudbase level and negative sensitivity from 850 to 450 hPa, which means that if the surrounding air in the boundary layer gets warmer and the mid-troposphere gets colder, there will be stronger convective activities and stronger cloud precipitation. For instance, if 1 ^oK positive θ perturbation occurs at the point with the largest gradient in the subcloud layer, it will induce an increase of about 9 mm/day in the overall precipitation rate. On the other hand, if this θ perturbation occurs at the point with the largest negative gradient around 500 hPa, it will result in about 14 mm/day decrease in total convective rain. This is due to the fact that warming up at lower level destabilizes the surrounding air and cooling down at upper level strengthens the cloud buoyancy force, which is measured by the difference between the moisture static energy in the cloud plume and the environment, thus favoring convective cloud development.

From 500 to 400 hPa, the gradient changes its sign from negative to positive, which indicates that precipitation is very sensitive to the vertical profile of temperature perturbations in mid-troposphere. For instance, if some heat source produces a positive θ perturbation at around 500 hPa, it tends to suppress convective activities as a whole, whereas if this perturbation occurs at a slightly higher level, say around 400 hPa, it will induce stronger convection and stronger precipitation.

The variation with height of the sensitivity of precipitation to moisture is displayed in Fig.2b. Only the levels below 850 hPa show significant positive sensitivity with the largest near 950 hPa, the cloudbase level. This means that more moisture near the cloud base level favors convective activities and induces stronger convective precipitation. Specifically, if a 1 g/kg perturbation in q occurs at the largest gradient point at 950 hPa, it tends to induce about 2.3 mm/day increase in total cloud precipitation. At upper levels around 450 hPa, there is a weak negative gradient, indicating opposite effects to these obtained at the lowest levels.

2) SENSITIVITY WITHIN A SINGLE COLUMN

From the former analysis, several representative grid points with high convective activities and high sensitivity are chosen to further analyze the sensitivity of R_θ and R_q in a single column. In the following three of them are discussed, which are:

- Point A: at $(100^0E, 6^0S)$ over the eastern Indian Ocean;
- Point B: at $(165^0W, 42^0N)$ over the mid-latitude Pacific ocean;
- Point C: at $(25^0E, 2^0S)$ over the tropical African continent.

Now the response functionals are defined as :

$$R_\theta = \Delta\theta(i, j, k)/\Delta t \qquad (12)$$

and

$$R_q = \Delta q(i,j,k)/\Delta t \tag{13}$$

where (i,j,k) indicates a particular grid point (i,j) at a particular vertical level k. Δt is the RAS time step. Since the RAS scheme is implemented columnwise, the output at a particular point at certain level can be sensitive to all the other vertical levels at this point, but not to the surrounding grid points. In a single column, the gradients of R_θ and R_q to environmental θ and q constitute the four component blocks of a Jacobian matrix, which is given by:

$$\begin{vmatrix} \nabla_\theta(R_\theta) & \nabla_q(R_\theta) \\ \nabla_\theta(R_q) & \nabla_q(R_q) \end{vmatrix} \tag{14}$$

Figs.3a to 3c display the four components of the Jacobian (14) at point A (100^0E, 6^0S). The ordinate is the σ level corresponding to k in R_θ in (12) and is directed from the surface upwards. They are referred to as the response levels. The abscissa consists of the σ levels of the surrounding air where perturbations occur, which are referred to as the influential levels. For example, the large negative value at point (0.5, 0.45) in Fig.3a provides the gradient of R_θ at the point (100^0E, 6^0S) at level $\sigma = 0.45$ (near 450 hPa) with respect to perturbations in θ at level $\sigma = 0.5$ (around 500 hPa).

From Figs.3a and 3b one can see that for R_θ, the level around 450 hPa displays the largest sensitivity, with positive gradient to both θ and q in the subcloud layers, where a 1^oK increase in θ leads to about $4^oK/day$ increase in cloud heating at 450 hPa level, whereas an additional 1 g/kg in the moisture content leads to about 8.7 $^oK/day$ increase in heating at 450 hPa level in terms of θ change. This impact is very significant. Fig.3a also shows a significant negative gradient with respect to θ near 500 hPa, where a 1^oK decrease in θ leads to a 5.6 $^oK/day$ increase in cloud heating rate at around 450 hPa. This implies a negative feedback between the θ perturbation in the environing air and the cloud-induced heating at around 450 hPa. However, at height 400 hPa a positive θ perturbation tends to enhance covective heating and the θ perturbation will grow, thus indicating a positive feedback.

The opposite impacts of perturbations occuring at 500 and 400 hPa on the convective heating can be explained by the fact that environmental heating is mainly accomplished by compensating downdrafts outside the clouds induced by the updrafts inside (Redelsperger and Guichard, 1996). Lower environmental air temperature in the mid-troposphere increases the difference of static energy between the cloud and the environment, thus increasing the buoyant force. This induces stronger updraft inside the cloud and downdraft outside it and stronger heating of the air column. On the other hand, if the layer around 400 hPa gets colder, the heating at the 450 hPa level through subsidence will be less effective. This explains the two opposite centers observed below and above 450 hPa in Fig.3a. The implication is that in order to accurately parameterize the cloud effects, an accurate vertical profile of the surrounding air is an essential prerequisite.

For R_q, the most influential layer is the subcloud layer (Figs.3c and d). The mid-level perturbation also can exert significant influence, however only on the adjacent layers. The layer around 500 to 600 hPa is significantly influenced by the θ and q perturbations in the surrounding air at the same level as well as at subcloud levels. A raise of 1^oK in temperature and $1g/kg$ in moisture content at subcloud layer tends to enhance convection, leading to a stronger convective drying of about 7×10^{-3} and 5×10^{-3} $(g/kg)/day$, respectively in the mid-troposphere (note from Fig1c that Δq is negative at most of the vertical levels). On the other hand, occurrence of positive θ and negative q perturbations at mid-troposphere around 600 hPa tends to suppress convective drying at the same level. Note the opposite effect of the q perturbations at $\sigma = 0.5$ (500 hPa) and $\sigma = 0.6$ (600 hPa) levels on the convective drying at 600 hPa. At around 600 hPa, the negative gradient implies that the feedback between the moisture perturbation and cloud drying effect is negative. The behavior of point A is typical of model gridpoint locations over low-latitude oceans with strong deep convective clouds.

Now we turn our attention to point B $(165^0W, 42^0N)$. Fig.4 shows the four components of the Jacobian at this point. Comparing Figs.4a and b with Figs.3a and b, one can see that for R_θ, the most sensitive response level is lowered to $\sigma = 0.5$ (around 500 hPa). This layer shows significant sensitivity to θ perturbations at the same level as well as at the levels below it. For R_q, Fig.4c and d shows that the most sensitive response level is even confined to below $\sigma = 0.8$ level. Negative θ and positive q perturbations between $\sigma = 0.8$ and $\sigma = 0.9$ (800 to 900 hPa) induce stronger convective drying. Also, the positive θ perturbation around $\sigma = 0.6$ level can lead to a suppression of convective drying at the layers lower than 850 hPa. This may be attributed to the reduced buoyancy force by higher environmental temperature.

The diagonal structure of the Jacobian, which is most evident in Fig.4d, indicates the local effect of the perturbations on convecting drying. The R_q at layers above 500 hPa shows little sensitivity to the θ and q perturbations at any level, probably since at high latitudes the convective clouds can not penetrate to very high levels, due to the fact that the moisture content in the air column is lower than that at low latitudes.

Fig.5 displays the Jacobian at grid point C $(25^0E, 2^0S)$. For R_θ, the major difference between the points C and A is that now the sensitivity of mid-troposphere R_θ to both θ and q disturbances is about an order of magnitude weaker (notice the difference in the contour intervals). Here the impact on convective heating from perturbations at mid- to upper troposphere is relatively more important than that from subcloud layers.

For R_q, Figs.5c and 5d show a marked difference compared to locations A and B. Now both the significantly sensitive layer and the influential layer are confined to below 900 hPa (notice the difference of the scale on the ordinate and abscissa between Figs.5c, d and the corresponding figures for points A and B). This is probably due to the presence of less moisture content in the air column and lower cloud top over land area than over low-latitude oceans. However Figs.5c and 5d still display detailed sensitivity structures with respect to the temperature and moisture perturbations, i.e. positive θ and q perturbations at the lowest model level and negative perturbations higher above (between 900 to 950 hPa) tend to destabilize the subcloud layers and strengthen convective drying. In fact at locations A and B such sensitivity structures at the lowest model levels are also observed. At the lowest model layers those points all depict strong negative feedback between q and the convective drying, whereas in the slightly higher layers, the feedback is positive.

From the above analysis of the three types of grid point locations we can conclude that as far as the perturbations are concerned, the conditions in the subcloud layers can most significantly influence the convective activities at each of these locations. For cloud effects at mid-troposphere, the influence from subcloud layer disturbances may surpass that arising from perturbations in the immediate surrounding air at the same level, especially for R_θ at grid points over the oceans. As to the response functions, the mid-troposphere is the one most easily influenced. The variations in cloud heating and drying effects are larger at these levels than at other levels if forced by the same perturbation. Over land and high latitude oceans, the moisture perturbation exhibits more localized effects which are mostly confined to the lowest model levels, whereas over the low latitude oceans with high sea surface temperature (SST) and stronger deep clouds, the impact of the boundary layer can be more readily transferred to higher levels.

Fillion and Errico (1997) also discussed the distribution of the blocks of the Jacobian at a single grid point location with strong convection, for both the Kuo and the RAS schemes (see their Figs.6 and 7). For the RAS scheme, they used the direct perturbation method instead of adjoint sensitivity to generate the Jacobian. They pointed out the influence from the lowest model layers, but their results show stronger upper-level diagonal structure which indicates a more localized effect. This difference from our results may be attributed to the choice of different time and geographic locations.

We can see that most of the layers display negative feedback between R_θ and the θ perturbation and between R_q and q perturbation. This suggests that perturbations in the environing air are suppressed by cloud activities. Therefore the cloud effect is by and large a stablizing factor for large-scale perturbations. However there are some vertical levels with positive feedback, to which more attention should be paid, since the interaction can cause rapid growth of the initial perturbations in the environing air.

b. Time-integrated sensitivity

The gradient of the time-integrated response is expected to yield a more stable and reliable sensitivity pattern than that of the instantaneous sensitivity. Moreover, it can provide us with the time evolution of the sensitivity. Now the matrix **S** in (1) is chosen such that the following two response functions are defined:

$$\begin{aligned} R_{\theta\theta} &= \int_{t_0}^{t_N} \sum_G \left(\frac{\partial\theta}{\partial t}\right)^2 dt \\ R_{qq} &= \int_{t_0}^{t_N} \sum_G \left(\frac{\partial q}{\partial t}\right)^2 dt \end{aligned} \tag{15}$$

Here $\sum_G$ reresents summation over the globe. These functionals provide a measure of the strength of the impact of convective clouds on the large-scale fields.

The integrations were carried out for 6 hours from 00 to 06GMT Jan. 1st, 1985. In this subsection the sensitivity (or gradient) to any variable actually means the sensitivity of the time-integrated response with respect to the perturbation of that variable at initial time.

1) SENSITIVITY TO POTENTIAL TEMPERATURE

Figs.6a and 6b display the longitude-height distribution of $R_{\theta\theta}$ and R_{qq} to θ perturbations, respectively, averaged in the latitudinal band between 10^0S and 10^0N. A major difference between these two figures and Fig.2a, which is the sensitivity of precipitation to θ, is that now all the levels above 700 hPa display negative gradients instead of a sharp change from negative to positive from 500 to 400 hPa. The most influential levels are to be found around 950 hPa and between 500 to 600 hPa, i.e. the perturbations occurring at these levels lead to larger variations in $R_{\theta\theta}$ than similar perturbations at other levels. Specifically, a 1 ^oK increase at subcloud layer or a 1 ^oK decrease around 500 hPa in θ leads to about $5 \times 10^{-6}\ ^oK^2/s$ increase and $2 \times 10^{-6}\ ^oK^2/s$ increase in $R_{\theta\theta}$, respectively.

Figs.6a and 6b also indicate that longitudinally the perturbations over the eastern Indian Ocean and the western Pacific Ocean exert the strongest influence on the convective heating and drying. However over the western Indian Ocean and the eastern Pacific Ocean, only the temperature perturbations under 800 hPa level can have significant impact.

In summary, the cloud impacts on the large-scale fields are most sensitive to the initial perturbations in θ field at two levels: one is the sub-cloud layer, the other is the mid-troposphere layer between 500 and 600 hPa. The perturbations at these layers have opposite effects on the convective parameterization, namely positive perturbations in the lower layers and negative perturbations in the upper layers lead to enhanced convective activities and to stronger impact on the environmental fields.

2) SENSITIVITY TO MOISTURE

Figs.7a and b show the vertical distribution of the sensitivity to moisture perturbations of $R_{\theta\theta}$ and R_{qq}, respectively, again averaged between $10^0 S$ and $10^0 N$. They are quite different from Fig.2b, which depicts the sensitivity of precipitation to the q perturbation. It is seen in Fig.7a that $R_{\theta\theta}$ displays a positive sensitivity to all the vertical levels, especially to the layers around 950 and 400 hPa, where a 1 g/kg increase in moisture content can result in 1 $\times 10^{-5}$ and 1.5 $\times 10^{-6}$ increase in $R_{\theta\theta}$, respectively, which means an increase in convective heating.

Fig.7b, which displays the R_{qq} sensitivity to moisture, shows a somewhat more complex behavior. Only the levels below 300 hPa are displayed since there is very little moisture above this level. The most significant positive gradient is observed around 950 hPa and 600 hPa. From 600 to 500 hPa, the gradient changes from large positive to negative. At around the 600 hPa layer, an addition of 1 g/kg in the moisture field results in about 2 $\times 10^{-7} (g/kg)^2/s$ increase in R_{qq}. On the contrary, adding 1 g/kg moisture at around 500 hPa tends to suppress convection (cf. Fig.2b) and reduce the convective drying effect, as manifested by about 1.5 $\times 10^{-7} (g/kg)^2/s$ decrease in R_{qq}.

This intricate structure is also manifest in Fig.3d but with reversed sign since in that figure, the response function is the Δq itself, which is negative, whereas in Fig.7b the response is the square sum of Δq, which is always positive.

From Fig.2b it can be seen that the q perturbation around 600 hPa does not significantly influence the strength of convection, which is represented there by convective precipitation, but here we observe that it can very significantly influence the convective drying. A possible explanation is that the convective drying in the environing air, like the convective heating, is mainly due to the compensating subsidence outside the clouds (Redelsperger and Guichard, 1996). This effect is most significant at around 600 hPa (Fig. 1c). Presence of additional moisture in the environing air at this level, will cause more water vapour to be transported to lower layers by downdrafts, thus leading to a larger depletion of moisture and larger negative Δq, even though the strength of convection does not increase significantly. If, on the other hand, there is additional moisture at higher levels, it tends to suppress convective activity (cf Fig.2b) so that the cloud-induced drying is reduced accordingly.

3) SENSITIVITY TO WIND FIELD

The wind fields do not exert an immediate impact on RAS scheme, so there is no instantaneous sensitivity to wind field. However the wind field redistributes the θ and q perturbations through advection and convergence/divergence. In this way it provides an indirect influence on the output of the RAS scheme. The integration of the adjoint model can provide us with the gradient of $R_{\theta\theta}$ and R_{qq} from RAS with respect to the wind field.

The vertical distribution of the gradient to zonal (u) and meridional (v) components of the wind field (figures omitted) both show a significant baroclinic structure with a vertical profile very similar to that of standing wave number 1. The node is at 500 hPa, with opposite signs below and above it. But within each regime, the structure exhibits a barotropic behavior. The two most influential levels are located near 750 hPa and 300 hPa, respectively.

By displaying the gradient of $R_{\theta\theta}$ with respect to u and v components in vector form, we obtain a concise view of the sensitivity to the perturbations in the wind vector. Figs.8a and b show the horizontal distribution of the sensitivity of $R_{\theta\theta}$ to the wind vector at 200 hPa and 700 hPa, which represents the situation at the upper and lower levels, respectively. The gradients of $R_{\theta\theta}$ at the two aforementioned layers have opposite signs, again indicating a baroclinic character. The most significant influence is due to the divergent component, whereas the vorticity component is very weak except at some isolated areas at high latitudes. The lower (upper) level gradient vector is largely convergent (divergent). The sensitivity to wind of R_{qq} is very similar to that of $R_{\theta\theta}$ and therefore is not shown here. As discussed in section 2, wind perturbations with the same structure and distribution, i.e. convergence at lower levels and divergence at upper levels over the convectively active regions at initial time, will lead to stronger cloud impacts on the environment in the ensuing several hours. The most sensitive region extends geographically from the eastern Indian Ocean to the western Pacific Ocean at low latitudes

c. Relative sensitivity of different variables

In the above we investigated the impacts of the perturbations in potential temperature, moisture and wind fields on the response functions. To provide an quantitative idea of the relative importance of each of these fields in causing the variation in the response functions, here we carry out a comparison contained in Table 2.

Considering the validity of the TLM and the adjoint sensitivity, small disturbances in the above fields are prescribed as shown in the first column of Table 2. Let us further suppose that each of these perturbations occurs at the most sensitive grid point for that variable (i.e. the point with the largest gradient). Table 2 lists the variations in the three response functionals resulting from each of the individual perturbations.

From Table 2 it can be seen that for the precipitation, θ is the most influential factor. Its impact is 2 to 3 times larger than that arising from q perturbations. For convective

Table 2: 1st order variations in response functionals

			$\delta R_p(mm/day)$	$\delta R_{\theta\theta}(^oK^2/s)$	$\delta R_{qq}(g^2/kg^2/s)$
$\delta\theta$	1×10^{-2}	^0K	1.4×10^{-1}	1.4×10^{-7}	2.2×10^{-9}
δq	1×10^{-2}	g/kg	5.0×10^{-2}	2.9×10^{-7}	5.0×10^{-9}
δW	1×10^{-2}	m/s		1.5×10^{-10}	1.0×10^{-10}

heating and drying, the q perturbation becomes the most influential factor although θ perturbation is almost as important. The variation caused by the wind perturbations is at least one order of magnitude smaller than that due to the θ and q perturbations, respectively.

5 Summary and Conclusions

Sensitivity of the RAS scheme in NASA's GEOS-1 GCM to perturbations in large-scale environmental fields was analyzed using the adjoint of the RAS parameterization scheme and the adiabatic GCM. The integrations of the adjoint model yield the gradients of the response functionals, which are measures of the strength of the cloud precipitation, the convective heating and convective drying effects, respectively, with respect to the perturbations of large-scale environmental fields. The most sensitive (in terms of the response functions) and the most influential (in terms of the large-scale perturbations) vertical levels are identified and the relative importance of the different variables is evaluated.

The results obtained show that the θ perturbation has a significant impact on all the response functionals analyzed, especially on the convective precipitation. The perturbations at subcloud layers and at mid-troposphere, from 500 to 600 hPa are found to be the most influential. The effects from lower layers and upper layers are opposite to each other, i.e. higher (lower) temperature perturbations at lower (upper) levels tend to produce positive variations to the response functions, indicating stronger convectivities and stronger cloud impact on the environing air.

The impact from moisture fields is most significant on the cloud heating and drying effects and the strongest influence comes from the subcloud layers, where additional moisture is conducive to stronger convective activities. The cloud-induced drying (moistening) is also significantly influenced by the moisture perturbations at mid-troposphere, with completely opposite effects from the 500 hPa compared to the 600 hPa disturbances, indicating a strong sensitivity of the response to grid-scale vertical profiles at mid-troposphere.

The regions where the perturbations are most effective in inducing variations in these response functions extends geographically from the eastern Indian Ocean to the western Pacific Ocean at low latitudes, where the convective activities are intense and frequent in a climatological sense.

The effects of the perturbations on convection are explained in terms of stability in the subcloud levels and the buoyancy force supporting cloud activities as well as the heat/moisture transport by convection.

The implications of these sensitivity analysis results are that accurate data of temperature, moisture and surface pressure are essential for an accurate evaluation of the cumulus cloud effects, especially at the most influential vertical levels which were identified above, since small perturbations at these locations tend to exert a stronger influence on the RAS outputs than the same perturbations at other locations.

The Jacobian of the cloud-induced $\Delta\theta$ and Δq to θ and q perturbations in a single air column, besides identifying the vertical levels of most sensitive response and most influential perturbations at various geographical locations, indicates the feedback of cloud activities on perturbations in the environing air. Most of the layers show negative feedback between convective heating and θ perturbations and between convective drying and moisture perturbations in the environment. However there are also some vertical layers in the mid-troposphere where the feedback is positive, indicating that the initial small perturbations can amplify through cloud effects.

Therefore, the above results should help to focus attention on data quality at those levels and areas with positive feedback between cloud activities and the environment, since small error tends to grow through this feedback.

The influence due to perturbations in the wind field is normally weaker than that due to perturbations in θ and q fields, but a reasonable sensitivity pattern was still obtained, namely convergence (divergence) at lower (upper) layers is favorable to convective activities and leads to a stronger cloud impact.

The results from the present work may also have important bearings on variational data assimilation, particularly the assimilation of precipitation data, in which moist convection is the dominant process. In variational assimilation of the precipitation data, the difference between model output rainfall and the observed rainfall (or the derivative of the cost function) is taken as input to the adjoint RAS scheme, and the output is the gradient of this cost function with respect to the large-scale variables. We may expect that the most influential levels identified in the present work are the ones most responsible for the reduction of the misfit, or the forecast error, which is represented by the cost function. In other words, these levels are the ones which experience the largest impact from observational data. This information can also be applied to the investigation of where additional adaptive observations should be taken.

We may expect that availability of better initial data in those sensitive areas and levels can also improve the model 'precipitation spin-up' during the first few hours of a numerical forecast. We intend to pursue this topic in our future research. Moreover, we are in the process of carrying out an adjoint sensitivity analysis of the moisture parameterization to some model parameters in order to provide us with some clues on ranking the most important parameters in the RAS package aiming at conducting optimal parameter estimation combined with 4-D variational data assimilation.

Acknowledgments The first and second authors acknowledge support by NASA grant NAG 5-1660 managed by Dr. Ken Bergman, section head of Climate Modeling, NASA headquarters. Thanks are due to Dr. Weiyu Yang at the Environmental Modeling Center, NCEP/UCAR for providing us with the adjoint codes used in this work which he developed when working with Prof. Navon at SCRI/Florida State University. We also thank Dr. Zhijin Li from SCRI/Florida State University for many fruitful discussions during the research. The data used in this work was obtained from the archived dataset in DAO/NASA. All the computations were carried out on NASA's CRAY J90. This research was also supported by Supercomputer Computations Research Institute at the Florida State University which is partially funded through contract DE-FC0583ER250000.

REFERENCES

Cacuci, D.G., 1981a: Sensitivity theory for nonlinear systems. *I*: Nonlinear functional analysis approach. *J. Math. Phys.*, **22**, 2794–2802.

Cacuci, D.G., 1981b: Sensitivity theory for nonlinear systems. *II*: Extensions to additional classes of responses. *J. Math. Phys.*, **22**, 2803-2812.

Cacuci, D.G., 1988: The forward and adjoint methods of sensitivity analysis. *Uncertainty Analysis*. Yigal Ronen. Ed., CRC Press, INC., 71-144.

Fillion, L. and R. Errico, 1997: Variational assimilation of precipitation data using moist convective parameterization schemes: A 1 D-var study. *Mon. Wea. Rev.,* **125**, 2917-2942.

Hall, M.C.G, 1986: Application of adjoint sensitivity theory to an atmospheric general circulation model. *J. Atmos. Sci.,* **43**, 2644-2651.

Hall, M.C.G, D.G. Cacuci and M. R. Schlesinger, 1982: Sensitivity analysis of a radiative-convective model by the adjoint method. *J. Atmos. Sci.,* **39**, 2038-2050.

Moorthi, S. and M.J. Suarez, 1992: Relaxed Arakawa-Schubert: A parameterization of moist convection for general circulation models. *Mon. Wea. Rev.,* **120**, 978–1002.

Navon, I. M., 1997: Practical and theoretical aspects of adjoint parameter estimation and identifiability in meteorology and oceanography. *Dyn. Atmos. Oceans,* **27**, 55-79.

Rabier, F. P. Courtier and O. Talagrand, 1992: An application of adjoint models to sensitivity analysis. *Beitr. Phys. Atmos.,* **65**, 177-192.

Rabier, F, E. Klinker, P. Courtier, and A. Hollingsworth, 1996: Sensitivity of forecast errors to initial conditions. *Quart. J. Roy. Meteor. Soc.,* **122**, 121–150.

Redelsperger, J. L. and F. Guichard, 1996: Detailed analysis of cloud systems observed during TOGA-COARE: simulations forced & unforced by the large scale motions. *New insights and approaches to convective parametrization. Proc. ECMWF Workshop*, Reading, United Kingdom, ECMWF, 58-76.

Rinne, J and H. Järvinnen, 1993: Estimation of the Cressman term for a barotropic model through optimisation with the use of the adjoint model. *Mon. Wea. Rev.,* **121**, 826-833.

Takacs, L.L., A. Molod, and T. Wang 1994: Documentation of the Goddard Earth Observing System (GEOS) general circulation model – Version 1. NASA Tech. Memo. 104606, Vol. 1.

Yang, W. and I.M. Navon, 1996: Documentation of the tangent linear model and its adjoint of the adiabatic version of the NASA GEOS-1 C-grid GCM - version 5.2. NASA Tech. Memo. 104606, Vol.8.

Yang, W., I.M. Navon, and R. Todling, 1997: Documentation of the tangent linear and adjoint models of the Relaxed Arakawa-Schubert moisture parameterization packages of the NASA GEOS-1 GCM (version 5.2). NASA Tech. Memo. 104606, Vol. 11.

Zou, X., A. Barcilon, I.M. Navon, J. Whitaker and D.G. Cacuci, 1993: An adjoint sensitivity study of blocking in a two-layer isentropic model. *Mon. Wea. Rev.*, **121**, 2833-2857.

CAPTIONS

Figure 1. Output from RAS scheme at 00GMT, Jan. 1st, 1985. a: convective cloud precipitation (interval 1.5 mm/day); b: cloud-induced change in potential temperature $\Delta\theta$ (interval 2.0×10^{-4} $^oK/s$); c: cloud-induced moisture change Δq (interval 1.0×10^{-4} $(g/kg)/s$). Shading indicates negative values. The ordinates in b and c are σ level.

Figure 2. Longitude-vertical distribution of the sensitivity of RAS precipitation to perturbations in (a) θ (interval 1.5, one unit corresponds to 2.0 $(mm/day)/^oK$) and (b) q (interval 1.0, one unit corresponds to 0.144 $(mm/day)/(g/kg)$). Shading indicates negative values. The ordinates are in hPa.

Figure 3. The four blocks of Jacobian at point $(100^0E, 6^0S)$. a: $\bigtriangledown_\theta(R_\theta)$, interval 0.5, one unit corresponds to 0.86 $(^oK/day)/^oK$; b: $\bigtriangledown_q(R_\theta)$, interval 2.0, one unit corresponds to 0.62 $(^oK/day)/(g/kg)$; c: $\bigtriangledown_\theta(R_q)$, interval 1.0, one unit corresponds to $1.2{\times}10^{-3}$ $(g/kg/day)/^oK$; d: $\bigtriangledown_q(R_q)$, interval 2.0, one unit corresponds to $0.86{\times}10^{-3}$ $(g/kg/day)/(g/kg)$.

Figure 4. Same as Fig.3 but for point $(165^0W, 42^0N)$ a: $\bigtriangledown_\theta(R_\theta)$, interval 0.5, one unit corresponds to 0.86 $(^oK/day)/^oK$; b: $\bigtriangledown_q(R_\theta)$, interval 1.5, one unit corresponds to 0.62 $(^oK/day)/(g/kg)$; c: $\bigtriangledown_\theta(R_q)$, interval 0.2, one unit corresponds to $1.2{\times}10^{-3}$ $(g/kg)/day/^oK$; d: $\bigtriangledown_q(R_q)$, interval 2.0, one unit corresponds to $0.86{\times}10^{-3}$ $(g/kg)/day/(g/kg)$.

Figure 5. Same as Fig.3 but for point $(25^0E, 2^0S)$ a: $\bigtriangledown_\theta(R_\theta)$, interval 0.05, one unit corresponds to 0.86 $(^oK/day)/^oK$; b: $\bigtriangledown_q(R_\theta)$, interval 0.1, one unit corresponds to 0.62 $(^oK/day)/(g/kg)$; c: $\bigtriangledown_\theta(R_q)$, interval 1.0, one unit corresponds to $1.2{\times}10^{-3}$ $(g/kg/day)/^oK$; d: $\bigtriangledown_q(R_q)$, interval 1.0, one unit corresponds to $0.86{\times}10^{-3}$ $(g/kg/day)/(g/kg)$.

Figure 6. Variations with longitude and height of the sensitivity to θ perturbations of the response (a) $R_{\theta\theta}$ (interval 0.5, one unit corresponds to 7.2×10^{-7} $(^oK^2/s)/^oK$) and (b) R_{qq} (interval 1.0, one unit corresponds to 1.4×10^{-8} $(g/kg)^2/s/^oK)$. Shading indicates negative values. The ordinates are in hPa.

Figure 7. Height-longitude distribution of sensitivity to moisture perturbations of the response (a) $R_{\theta\theta}$ (interval 1.0, one unit corresponds to 5.18×10^{-7} $(^oK^2/s)/(g/kg)$) and (b) R_{qq} (interval 0.2, one unit corresponds to 1.0×10^{-7} $(g/kg)^2/s/(g/kg)$). Shading indicates negative values. The ordinates are in hPa.

Figure 8. Sensitivity of $R_{\theta\theta}$ response to perturbations in wind vector at (a) 200 hPa and (b) 700 hPa. one unit corresponds to 5.2×10^{-10} $(^oK^2/s)/(m/s)$

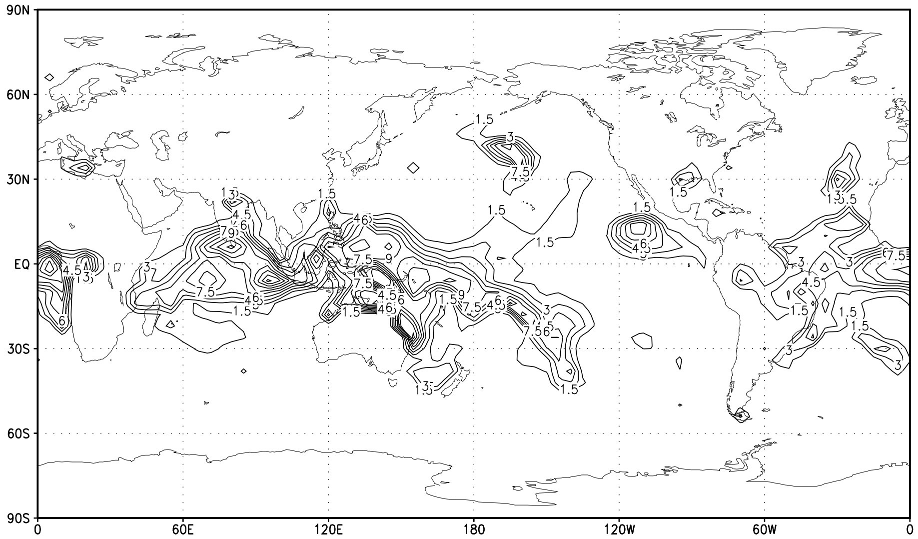

1 (a)

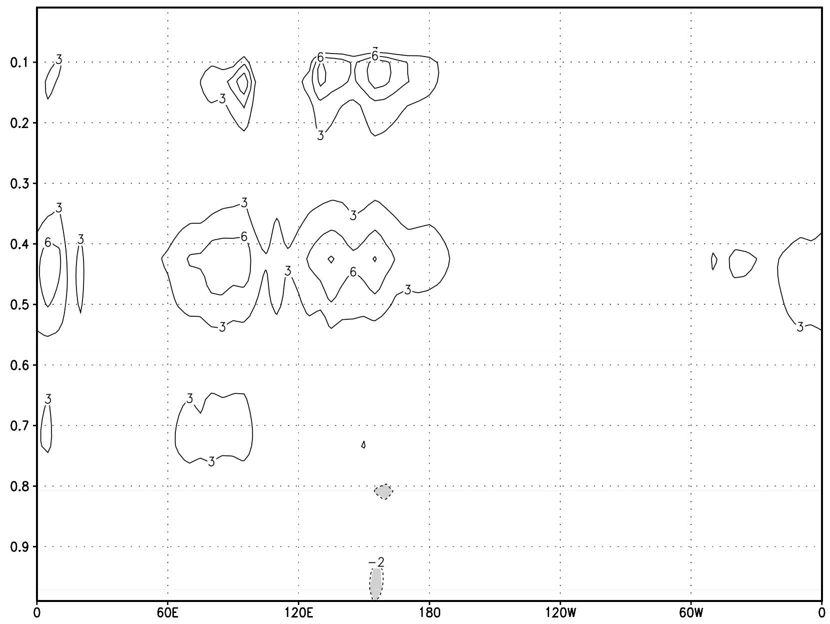

1 (b)

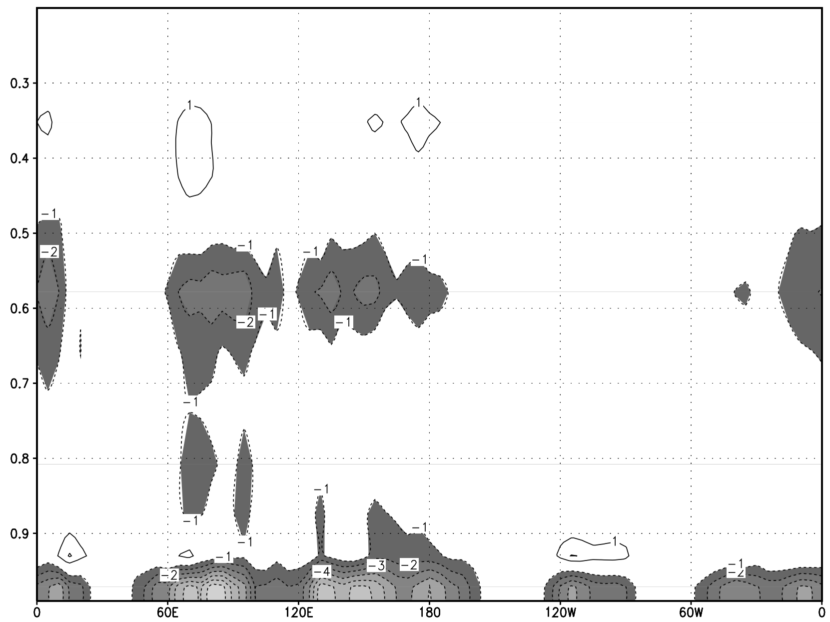

1 (c)

Figure 1: Output from RAS scheme at 00GMT, Jan. 1st, 1985. a: convective cloud precipitation (interval 1.5 mm/day); b: cloud-induced change in potential temperature $\Delta\theta$ (interval $2.0 \times 10^{-4}\ ^{o}K/s$); c: cloud-induced moisture change Δq (interval $1.0 \times 10^{-4}\ (g/kg)/s$). Shading indicates negative values. The ordinates in b and c are σ level.

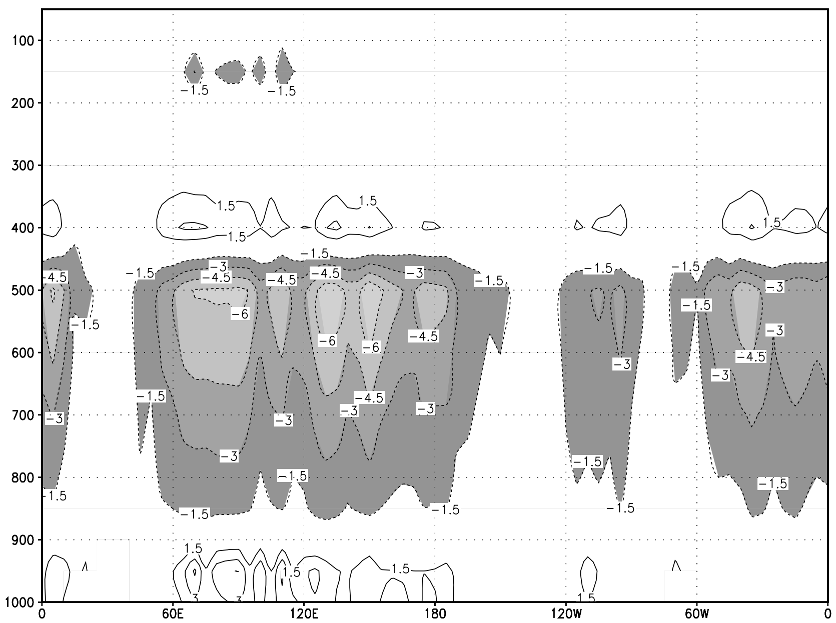

(a)

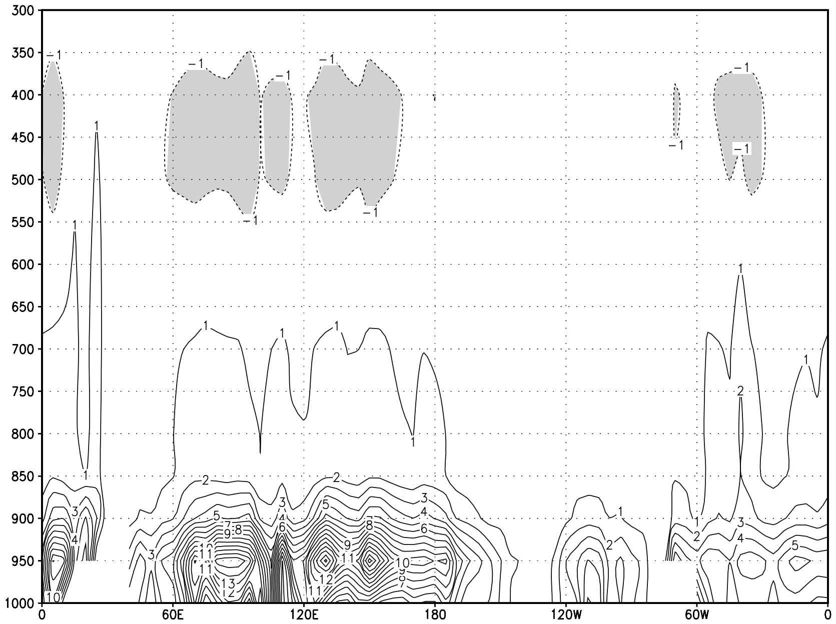

(b)

Figure 2: Longitude-vertical distribution of the sensitivity of RAS precipitation to perturbations in (a) θ (interval 1.5, one unit corresponds to 2.0 $(mm/day)/^oK$) and (b) q (interval 1.0, one unit corresponds to 0.144 $(mm/day)/(g/kg)$). Shading indicates negative values. The ordinates are in hPa.

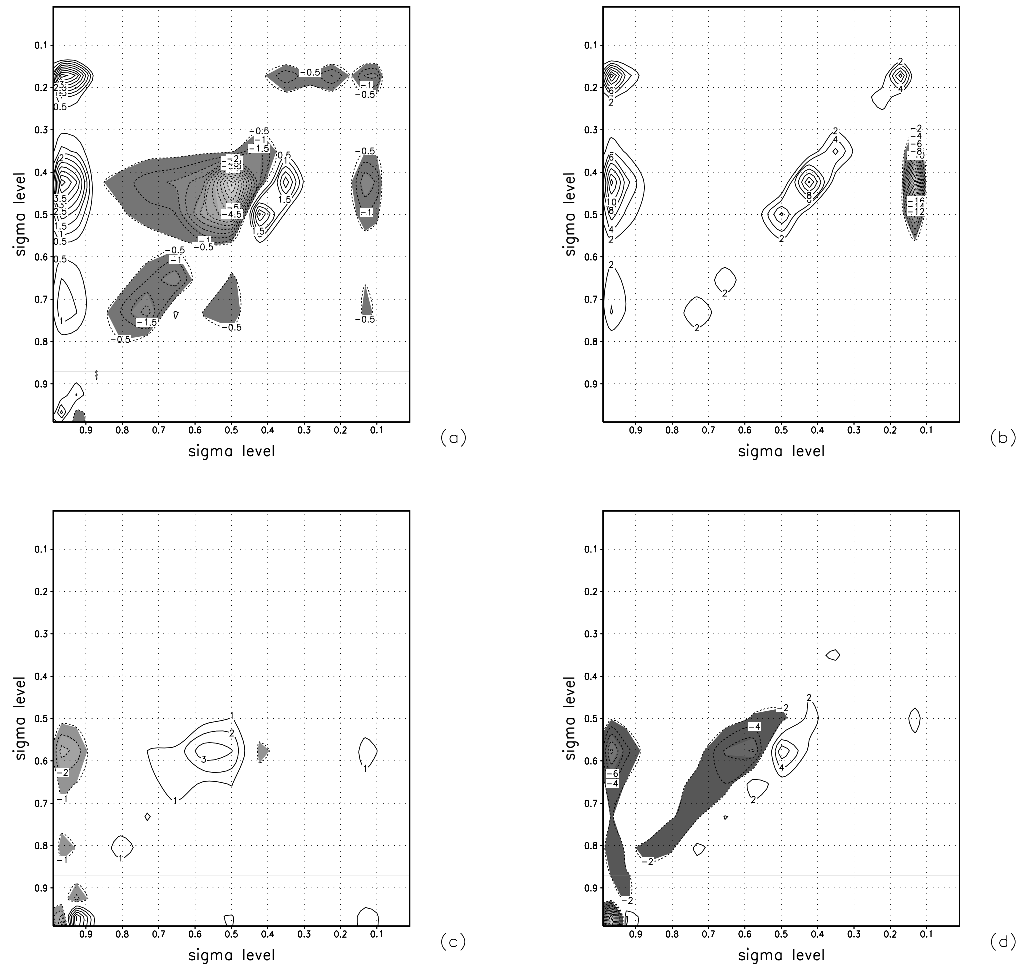

Figure 3: The four blocks of Jacobian at point $(100^0E, 6^0S)$. a: $\bigtriangledown_\theta(R_\theta)$, interval 0.5, one unit corresponds to 0.86 $(^oK/day)/^oK$; b: $\bigtriangledown_q(R_\theta)$, interval 2.0, one unit corresponds to 0.62 $(^oK/day)/(g/kg)$; c: $\bigtriangledown_\theta(R_q)$, interval 1.0, one unit corresponds to 1.2×10^{-3} $(g/kg/day)/^oK$; d: $\bigtriangledown_q(R_q)$, interval 2.0, one unit corresponds to 0.86×10^{-3} $(g/kg/day)/(g/kg)$. Shading indicates negative values.

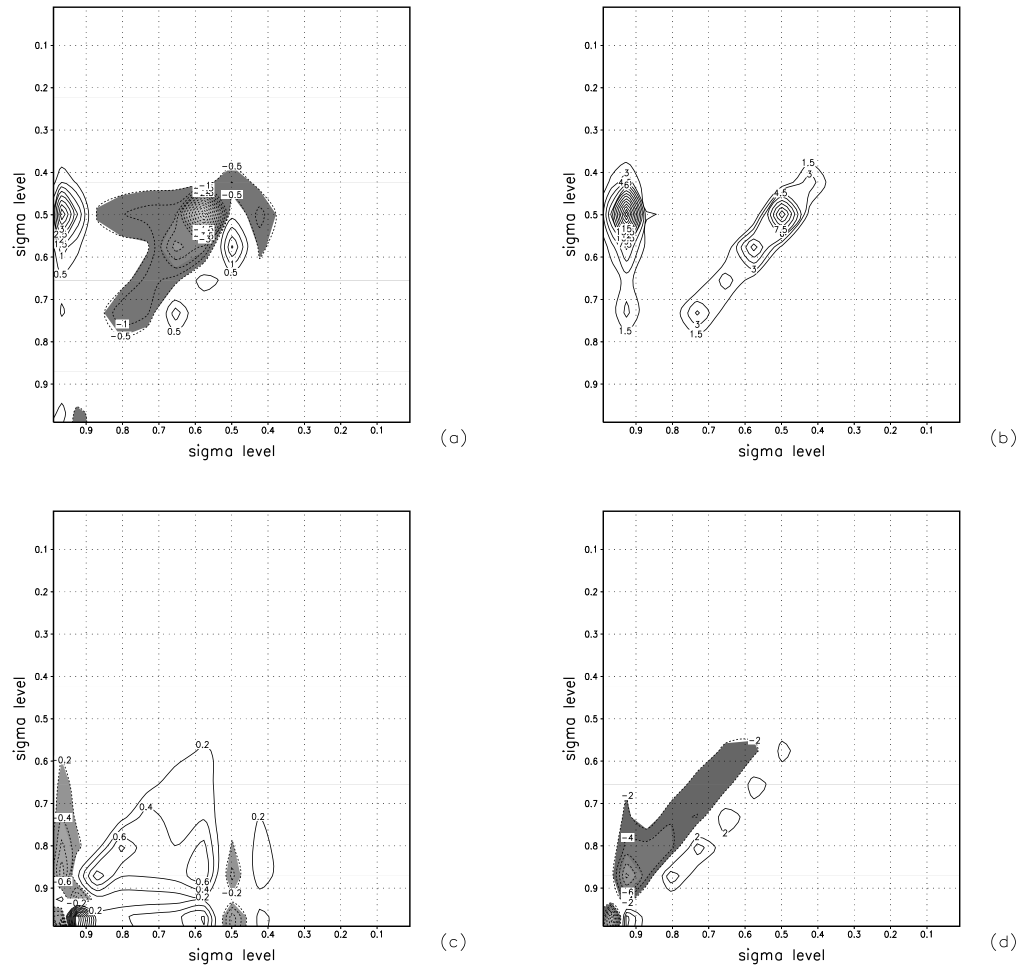

Figure 4: Same as Fig.3 but for point $(165^0W, 42^0N)$ a: $\bigtriangledown_\theta(R_\theta)$, interval 0.5, one unit corresponds to 0.86 $(^oK/day)/^oK$; b: $\bigtriangledown_q(R_\theta)$, interval 1.5, one unit corresponds to 0.62 $(^oK/day)/(g/kg)$; c: $\bigtriangledown_\theta(R_q)$, interval 0.2, one unit corresponds to 1.2×10^{-3} $(g/kg)/day/^oK$; d: $\bigtriangledown_q(R_q)$, interval 2.0, one unit corresponds to 0.86×10^{-3} $(g/kg)/day/(g/kg)$. Shading indicates negative values.

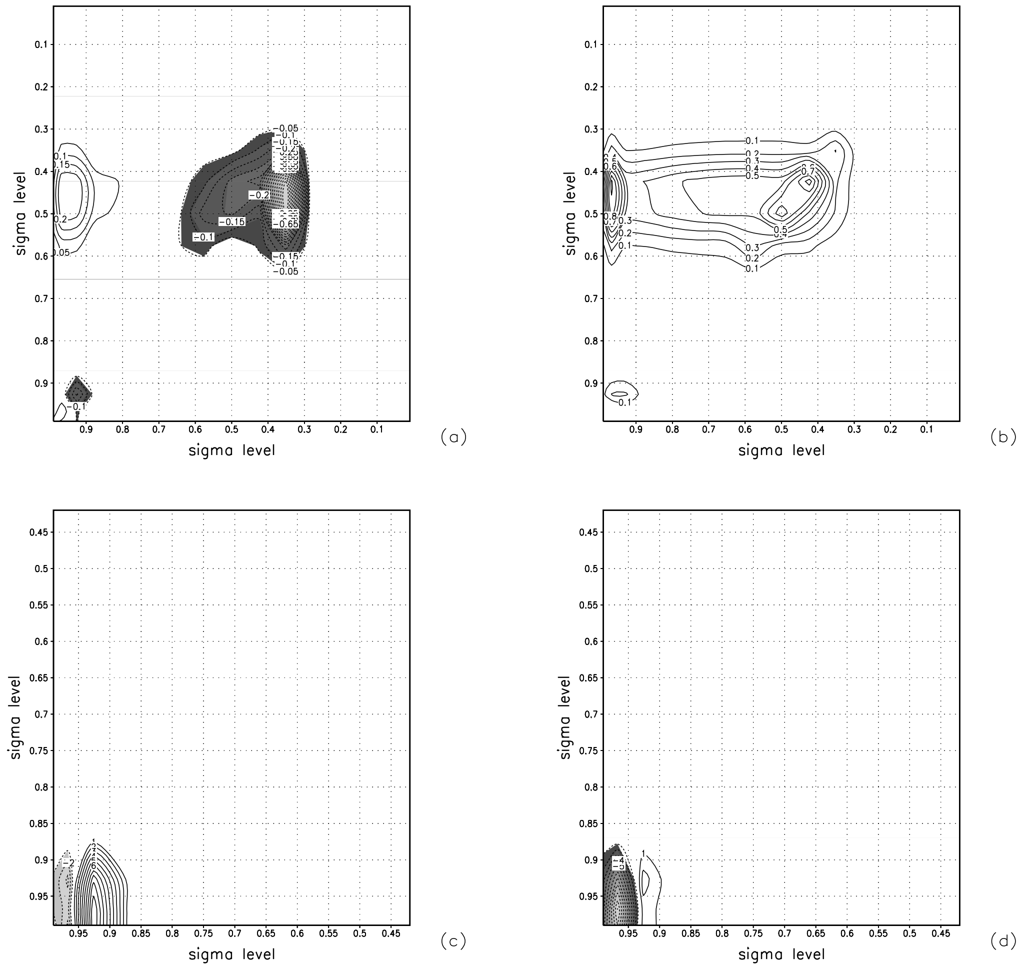

Figure 5: Same as Fig.3 but for point $(25^0E, 2^0S)$ a: $\bigtriangledown_\theta(R_\theta)$, interval 0.05, one unit corresponds to 0.86 $(^oK/day)/^oK$; b: $\bigtriangledown_q(R_\theta)$, interval 0.1, one unit corresponds to 0.62 $(^oK/day)/(g/kg)$; c: $\bigtriangledown_\theta(R_q)$, interval 1.0, one unit corresponds to 1.2×10^{-3} $(g/kg/day)/^oK$; d: $\bigtriangledown_q(R_q)$, interval 1.0, one unit corresponds to 0.86×10^{-3} $(g/kg/day)/(g/kg)$. Shading indicates negative values.

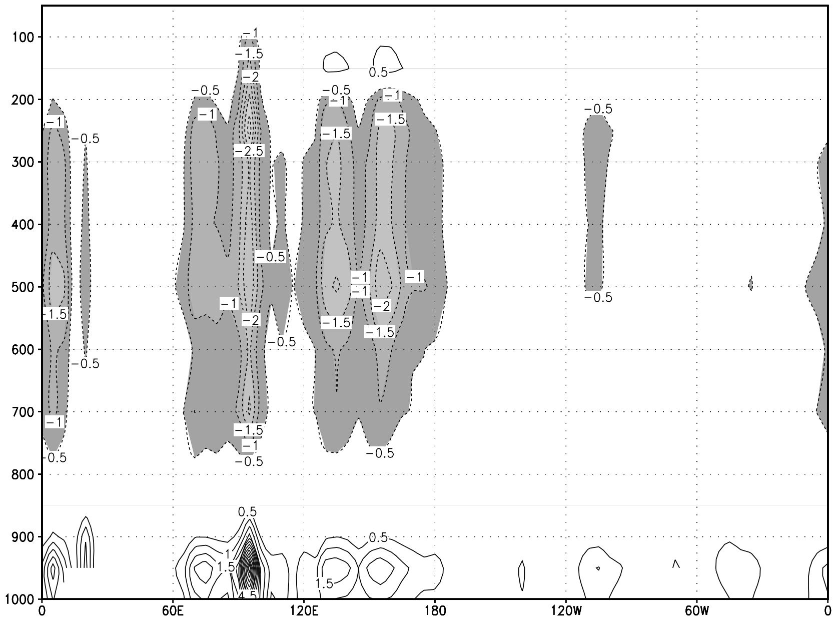

(a)

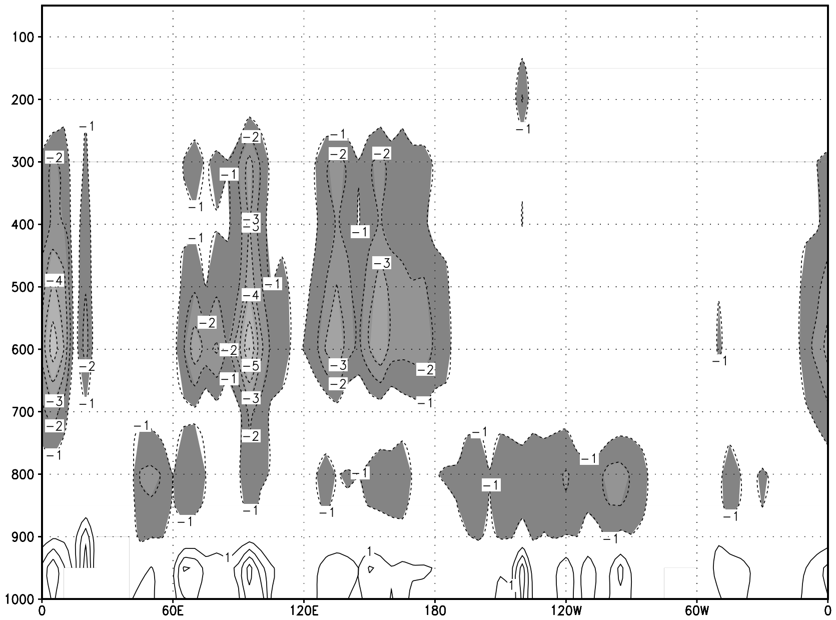

(b)

Figure 6: Variations with longitude and height of the sensitivity to θ perturbations of the response (a) $R_{\theta\theta}$ (interval 0.5, one unit corresponds to 7.2×10^{-7} $(^oK^2/s)/^oK$) and (b) R_{qq} (interval 1.0, one unit corresponds to 1.4×10^{-8} $(g/kg)^2/s/^oK$). Shading indicates negative values. The ordinates are in hPa.

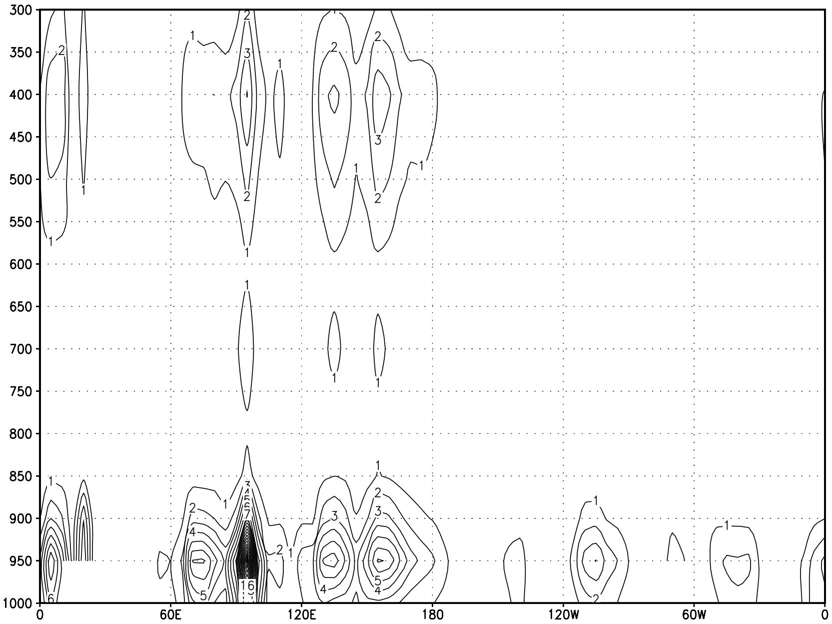

(a)

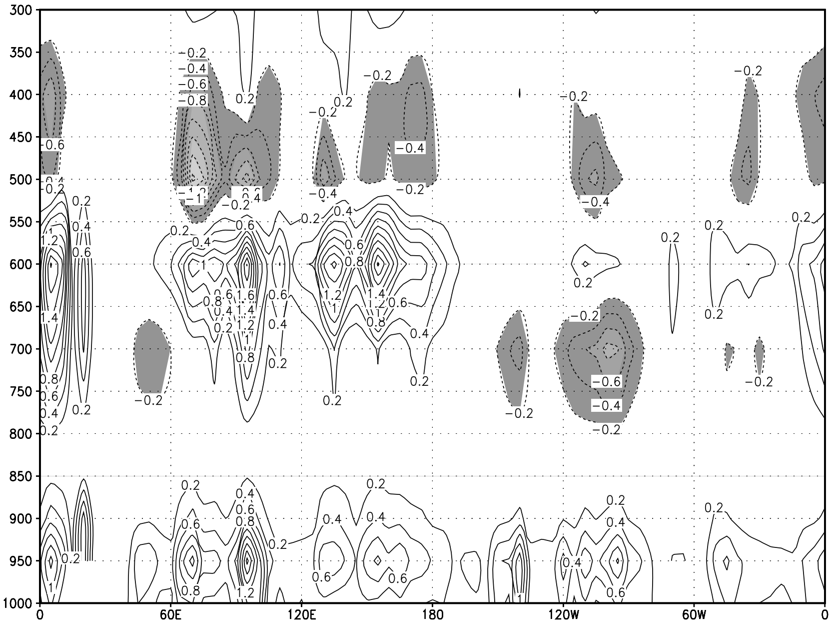

(b)

Figure 7: Height-longitude distribution of sensitivity to moisture perturbations of the response (a) $R_{\theta\theta}$ (interval 1.0, one unit corresponds to 5.18×10^{-7} $(^oK^2/s)/(g/kg)$) and (b) R_{qq} (interval 0.2, one unit corresponds to 1.0×10^{-7} $(g/kg)^2/s/(g/kg)$). Shading indicates negative values. The ordinates are in hPa.

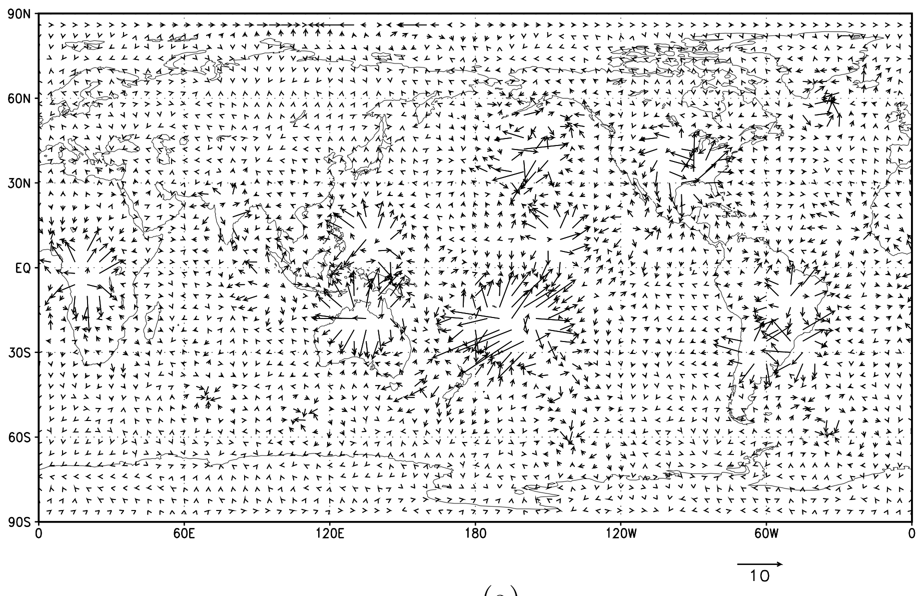

(a)

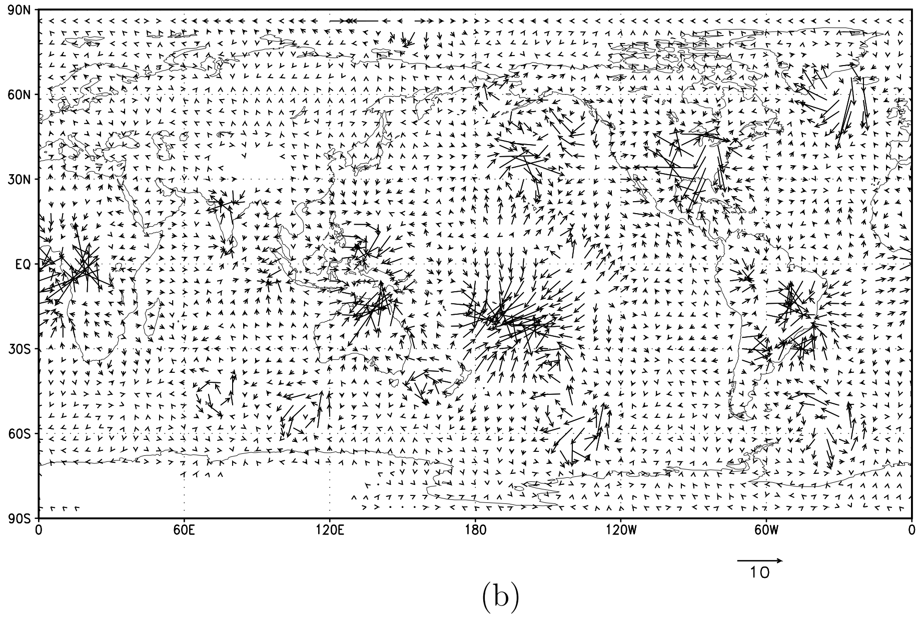

(b)

Figure 8: Sensitivity of $R_{\theta\theta}$ response to perturbations in wind vector at (a) 200 hPa and (b) 700 hPa. one unit corresponds to 5.2×10^{-10} $(^{o}K^{2}/s)/(m/s)$